Nuclear Resonance Vibrational Spectroscopy and Electron Paramagnetic Resonance Spectroscopy of ^{57}Fe-Enriched [FeFe] Hydrogenase Indicate Stepwise Assembly of the H-Cluster

Jon M. Kuchenreuther,[£,∂] Yisong Guo,[§] Hongxin Wang,[£,‡] William K. Myers,[£] Simon J. George,[£] Christine A. Boyke,[¶] Yoshitaka Yoda,[¥] E. Ercan Alp,[Δ] Jiyong Zhao,[Δ] R. David Britt,[£] James R. Swartz,[∂,ß] and Stephen P. Cramer[£,‡]

[£] *Department of Chemistry, University of California, Davis, CA 95616*

[∂] *Department of Chemical Engineering, Stanford University, Stanford, CA 94305*

[§] *Department of Applied Science, University of California, Davis, CA 95616*

[‡] *Physical Biosciences Division, Lawrence Berkeley National Laboratory, Berkeley, CA 94720*

[¶] *Department of Chemistry, University of Illinois, Champagne-Urbana, IL 61801*

[¥] *JASRI, SPring-8, 1-1-1 Kouto, Sayo-cho, Sayo-gun, Hyogo 679-5198, Japan*

[Δ] *Advanced Photon Source, Argonne National Laboratory, Argonne, IL 60439*

[ß] *Department of Bioengineering, Stanford University, Stanford, CA 94305*

Supporting Information

Experimental Methods

Synthesis of the ^{57}Fe-labeled $[2Fe]_H$ subcluster biomimetic complex. Published methods were used for the synthesis of $(Et_4N)_2[^{57}Fe_2(S_2C_3H_6)(CN)_2(CO)_4]$[1,2] as well as the ^{13}CN-substituted complex.[3,4] Synthetic compounds were isotopically enriched using $^{57}FeCl_2$, and both NRVS and FTIR spectroscopy were carried out on the same samples.

DFT calculations. The BP86 functional was used for all calculations of the $[Fe_2(S_2C_3H_6)(CO)_4(CN)_2]^{2-}$ model complex,[5,6] as implemented in the Gaussian 09 software package.[7] A triple-zeta basis set with polarization functions (TZVP) was used for all of the atoms.[8,9] The initial structural model for $[Fe_2(S_2C_3H_6)(CO)_4(CN)_2]^{2-}$ was taken from the published crystal structure.[2] The SCF procedure and geometry optimization were terminated upon reaching the default convergence criteria.

FTIR spectroscopy. IR spectra for the model complex were recorded at room temperature using a Bruker IFS 66 v/S FTIR spectrometer. The sample chamber was maintained at 1 torr to minimize absorption by water vapor. The scanning speed was 10 kHz, and the energy resolution was 4 cm^{-1}. Measurements were performed with different combinations of beamsplitters, detectors, sample preparations, and sample cell windows to optimize within each wavelength region. Samples for measurements in the far-IR region (350–700 cm^{-1}) were prepared in the form of a KBr mixture sealed with polyethylene windows and measured with a KBr beamsplitter and a Si bolometer. For the mid-IR region (1750–2150 cm^{-1}), measurements were done using a KBr beamsplitter, a MCT detector, KBr as the sample medium material, and ZnSe windows.

Results and Discussion

The $(Et_4N)_2[Fe_2(S_2C_3H_6)(CN)_2(CO)_4]$ complex: a model compound of the [FeFe] hydrogenase $[2Fe]_H$ subcluster. The $[Fe_2(S_2C_3H_6)(CN)_2(CO)_4]^{2-}$ model compound contains two low spin Fe^I atoms, with each atom embedded in a square pyramidal geometry. Each Fe center is coordinated with two terminal CO molecules and one terminal CN^- molecule. One CN^- occupies the axial position (CN_{ax}) of the square pyramid on one Fe center (Fe_1), and the other CN^- occupies a basal position (CN_{bas}) on the other Fe center (Fe_2). The two Fe atoms are linked by two S atoms via a 1,3-propane dithiolate bridging ligand ($S_2C_3H_6$) that is commonly notated as "pdt." As illustrated in Figure S1, the compound provides a reasonable structure model for the [FeFe] hydrogenase $[2Fe]_H$ subcluster in the reduced state (H_{red}).[2] We have performed FTIR spectroscopy, NRVS, and DFT calculations on the ^{57}Fe-enriched model complex containing either natural abundance CN^- ligands or isotopically labeled $^{13}CN^-$ ligands in order to explore its molecular vibrations, and in particular, the vibrational modes associated with the Fe–CO and Fe–CN moieties. The results are used to interpret the NRVS results for the CpI hydrogenase containing an ^{57}Fe-enriched $[2Fe]_H$ subcluster.

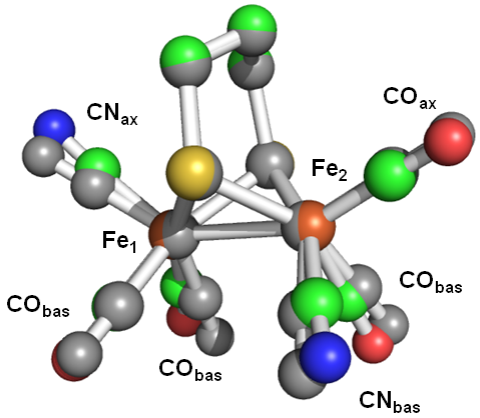

Figure S1. Structure overlap of the crystal structure (shown in gray) and the DFT-optimized structure of the $[Fe_2(S_2C_3H_6)(CN)_2(CO)_4]^{2-}$ model compound. The following color scheme was used for the DFT-based structure: Fe (brown), S (yellow), C (green), O (red), and N (blue). Hydrogen atoms are omitted for clarity.

DFT calculations. To assist with our analysis of the FTIR spectroscopy and NRVS data, DFT calculations were performed on the model complex. The DFT-optimized structure of the model complex, which closely resembles the crystal structure (Figure S1), was used for frequency calculations and the generation of the IR intensities as implemented in Gaussian 09 (Figure S2). Calculated NRVS modes shown in Figure S3 were determined using an in-house program that analyzes the Cartesian normal mode displacements calculated by Gaussian 09. To mimic the experimental resolution, the DFT spectra were generated by using a convoluation of the stick intensities with 9 cm^{-1} broadening. Several key geometric parameters are listed in Table S1. Herein, we use the ligand nomenclature indicated in Figure S1 to describe the normal modes identified by the DFT calculations.

Table S1. Selected structure parameters for the $[Fe_2(S_2C_3H_6)(CN)_2(CO)_4]^{2-}$ model complex.

	Bond Length (Å)			Bond Angles (°)	
Bonds	*X-ray*[a]	*DFT*	**Bonds**	*X-ray*[a]	*DFT*
Fe–Fe	2.52	2.60	Fe–S–Fe[b]	67	69
$Fe–CN_{ax}$	1.92	1.92	S–Fe–S[b]	86	86
$Fe–CN_{bas}$	1.94	1.92	$CO_{ax}–Fe–CO_{bas}$	99	101
$Fe–CO_{bas}$	1.77	1.75	$CO_{bas}–Fe–CO_{bas}$	93	91
$Fe–CO_{eq}$	1.74	1.75	$CN_{ax}–Fe–CO_{bas}$[b]	102	99
Fe–S	2.28	2.31	$CN_{bas}–Fe–CO_{ax}$	99	94
			$CN_{bas}–Fe–CO_{bas}$	91	88

[a]Values obtained from the crystal structure.[1]

[b]Averaged values.

FTIR spectroscopy and DFT calculations in the mid-IR region for the $[Fe_2(S_2C_3H_6)(CN)_2(CO)_4]^{2-}$ complex. Figure S2 shows the FTIR spectra for the model complex in the mid-IR region (1750–2150 cm^{-1}). Six absorption features were identified. Furthermore, the DFT results resemble the experimental data reasonably well, and numbers in parentheses refer to the DFT-calculated energies.

The two higher-energy peaks are located at 2075 (2070; CN_{ax}) and 2026 (2089; CN_{bas}) cm^{-1}, which are within the region where CN^- stretching modes (ν(CN)) are typically observed. Upon $^{13}CN^-$ labeling of the model complex, these two peaks shift to lower frequencies, specifically to 2030 (2026) and 1984 (2044) cm^{-1}, confirming the assignment of these peaks as ν(CN) stretching modes. The isotope shifts are in close agreement with those expected when considering Hooke's Law for a diatomic harmonic oscillator, which predicts a shift of 44 cm^{-1} following ^{13}C-substitution in the CN^- ligands.

In the lower-energy region (1750–2000 cm^{-1}), four strong absorption features are located at 1873 (1857), 1889 (1878), 1923 (1906), and 1962 (1941) cm^{-1}. These bands are characteristic of CO stretching modes (ν(CO)). Our assignment of these peaks as ν(CO) stretches is supported by the absence of a shift in their frequencies for the ^{13}CN-labeled model complex.

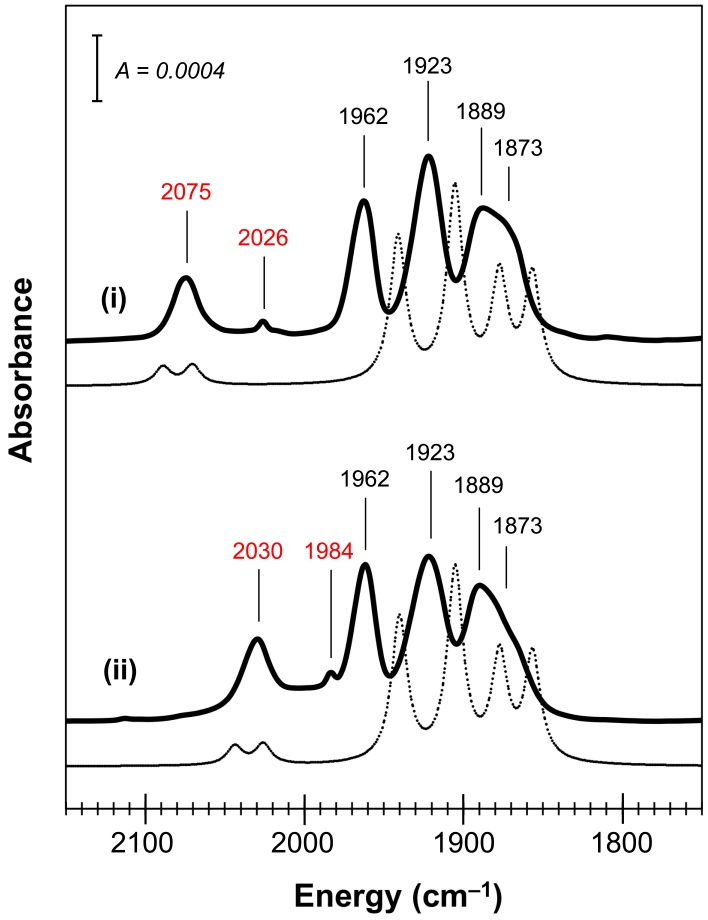

Figure S2. FTIR spectroscopy and DFT results for the $[Fe_2(S_2C_3H_6)(CN)_2(CO)_4]^{2-}$ model compound. Spectra show the ν(CO) and ν(CN) vibrational bands in the mid-IR region for (**i**) the model complex and (**ii**) the ^{13}CN-labeled model complex. Solid lines represent the measured IR spectra, and dashed lines represent the DFT-calculated IR spectra. Peak energies for the measured data are provided. Energies for peaks that were sensitive to isotopic labeling with ^{13}CN are assigned to ν(CN) stretches and are shown in red font type. The vertical scale bar pertains to the experimental FTIR spectroscopic intensities.

NRVS, FTIR, and DFT-based spectra for the $[Fe_2(S_2C_3H_6)(CN)_2(CO)_4]^{2-}$ model complex in the far-IR region. Figure S3 shows the NRVS vibrational density of states, the FTIR spectra, and the DFT-based results for the model complex in the far-IR region, specifically in the region in which Fe–CO and Fe–CN vibrations are expected (350–700 cm^{-1}). Similar to the results within the mid-IR region, the DFT results within the far–IR region resemble the NRVS and FTIR measured data reasonably well, and again, numbers in parentheses refer to the DFT-calculated energies.

The Fe–CN stretching modes (ν(Fe–CN)) and Fe–CN bending modes (δ(Fe–CN)) are expected to be in the 350–450 cm^{-1} region. For the model compound, Brunold and co-workers assigned Raman features at 432 and 450 cm^{-1} to ν(Fe–CN) stretching modes, and a feature at 390 cm^{-1} to a δ(Fe–CN) bending mode.[4] In the NRVS spectra, two strong features were observed at 418 (413) and 440 (438) cm^{-1} for the complex with natural abundance CN^-. This set of bands downshifts ~18 cm^{-1} to 400 (408) and 422 (429) cm^{-1} following ^{13}CN-substitution, indicating that these features are from Fe–CN vibrations. The normal modes responsible for these two features are mainly from a mixture of ν(Fe–CN) stretches and δ(Fe–CN) bends along with some coupling to Fe–CO vibrations. For example, the 413 cm^{-1} band is a combination of the $\nu(Fe_1–CN_{ax})$ stretch and the $\delta(Fe_2–CN_{bas})$ bend as determined from our DFT calculations. The relatively pure δ(Fe–CN) bending modes are calculated to exist from 375 to 400 cm^{-1}, which give almost no ^{57}Fe PVDOS intensities. Regarding the FTIR spectroscopic results, two relatively strong IR features are located at 384 and 403 cm^{-1}, which respectively downshift to 372 and 398 cm^{-1} upon ^{13}CN-labeling. The observed changes in these IR features following isotopic labeling indicate they are from Fe–CN vibrations. Interestingly, no CN peaks in the IR spectra match those in the NRVS spectra, and no CN peaks in the NRVS spectra match those in the IR spectra. Differences in intensity mechanisms between NRVS and FTIR spectroscopy most likely account for this result. Furthermore, the DFT-calculated bands at 413 and 438 cm^{-1} give weak IR intensities, and the calculated δ(Fe–CN) bending modes between 375–400 cm^{-1} give even weaker IR intensities.

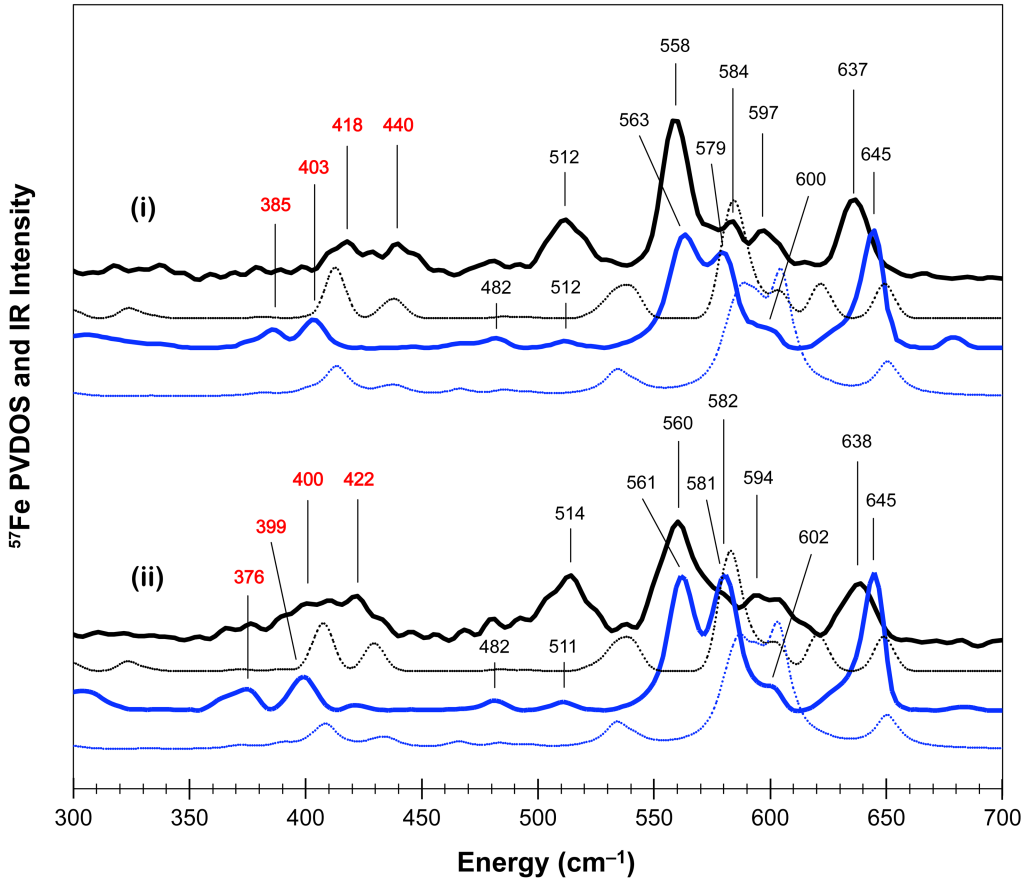

Figure S3. NRVS PVDOS, FTIR spectroscopy, and DFT results for (**i**) the $[Fe_2(S_2C_3H_6)(CN)_2(CO)_4]^{2-}$ complex and (**ii**) the isotopically ^{13}CN-labeled $[Fe_2(S_2C_3H_6)(^{13}CN)_2(CO)_4]^{2-}$ complex. Spectra show the 350–700 cm^{-1} region in which Fe–CO and Fe–CO modes are expected. The black and blue curves represent the NRVS and FTIR spectra, respectively. Solid lines and dashed lines represent the experimental and DFT results, respectively. Peak energies for the experimental data are provided. Energies for peaks that were sensitive to isotopic labeling with ^{13}CN are assigned to Fe–CN modes and are shown in red font type.

Multiple strong and weak features between 450–650 cm^{-1} are shown in the NRVS-based PVDOS and FTIR spectra for the model complex. All NRVS and IR features within this region show very small shifts in energy following $^{13}CN^-$ labeling, which supports their assignments as Fe–CO vibrations. Based on our DFT calculations as well as previous spectroscopic studies of iron compounds with CO moieties,[10,11] the lower-energy features between 450–650 cm^{-1} are primarily Fe–CO stretching modes (ν(FeCO)), while the higher-energy features are primarily Fe–CO bending modes (δ(FeCO)). At the low end of this region, a strong PVDOS feature is located at 512 (538) cm^{-1}, with a corresponding weak IR feature at 512 (534) cm^{-1}. This band is mainly from two normal modes, which are in-phase and out-of-phase symmetric ν_{sym}(Fe–CO) stretches involving both the Fe_1–(*cis*-CO_{bas})$_2$ and Fe_2–(*cis*-$CO_{bas/ax}$)$_2$ moieties. The strongest peak is located at 558 (585) cm^{-1} with a corresponding IR feature at 563 (589) cm^{-1}. This band consists of four normal modes based on our DFT calculations. Two of these modes give strong PVDOS and IR intensities, which are mainly asymmetric ν_{asym}(Fe–CO) stretches from either the Fe_1–(*cis*-CO_{bas})$_2$ or the Fe_2–(*cis*-$CO_{bas/ax}$)$_2$ moieties, and which are located at 588 and 583 cm^{-1}. Relatively weaker shoulders are located at 584 (603) and 597 (622) cm^{-1} in the NRVS spectra, with a strong corresponding IR band at 579 (604) cm^{-1} and a weak IR band at 602 cm^{-1}. The DFT-calculated feature at 604 cm^{-1} gives strong IR intensity, yet weak ^{57}Fe PVDOS intensity, which is attributed to an in-phase and out-of-plane δ(Fe–CO) bending mode that involves both Fe_1–(*cis*-CO_{bas})$_2$ and Fe_2–(*cis*-$CO_{bas/ax}$)$_2$ moieties. The highest energy peak in both DFT-calculated spectra is a rather pure in-plane δ(Fe–CO) bend from the Fe_1–(*cis*-CO_{bas})$_2$ moiety, which is observed as a 637 (649) cm^{-1} PVDOS peak that matches up with a strong IR feature at 645 (651) cm^{-1}.

It is noteworthy that, when compared with the corresponding Fe–CO vibrations and ν(CO) stretches/bends, the lower-energy Fe–CN vibrations together with the higher-energy ν(CN) stretches (relative to the bends) are consistent with the weaker π back-bonding interactions between Fe and CN^- than those interactions between Fe and CO. This is also reflected by the Fe–CN bond lengths, which are ~0.2 Å longer than the Fe–CO bond lengths in the model compound crystal structure.

In summary, with the help of IR spectroscopy and DFT calculations, the NRVS vibrational density of states for the model complex have been clearly assigned as either Fe–CO or Fe–CN vibrations. Based on our DFT calculations, the Fe–CO modes are observed from 450 to 650 cm^{-1}, with ν(Fe–CO) stretching vibrations located at lower energies and the δ(Fe–CO) bending vibrations located at higher energies. The Fe–CN vibrations are observed from 350 to 450 cm^{-1}, and they were identified as such given the shifts in energies following ^{13}CN substitution. Furthermore, the δ(Fe–CN) bending modes are located from 350 to 400 cm^{-1}, while the peaks from 400 to 450 cm^{-1} are primarily from a mixture of ν(Fe–CN) stretches and δ(Fe–CN) bends, along with some coupling of these modes to Fe–CO vibrational modes.

NRVS of the CpI hydrogenase, the $[Fe_2(S_2C_3H_6)(CN)_2(CO)_4]^{2-}$ compound, and a [4Fe–4S] ferredoxin. Two independent $CpI^{[57Fe]H}$ samples were prepared and measured with NRVS. The resulting ^{57}Fe PVDOS are presented in Figure S4 and are compared to those for the model compound as well as the published NRVS results for the *Pyrococcus furiosus* [4Fe–4S] ferredoxin (*Pf* D14C Fd variant).[12] Table S2 summarizes the total intensity within the regions where Fe–S vibrations as well as Fe–CO/Fe–CN vibrations are observed as determined by calculating the area under the curves.

This work represents the first NRVS of [FeFe] hydrogenases. Therefore, we have tentatively assigned selected features based on our comparisons of the hydrogenase results to the model compound and [4Fe–4S] ferredoxin results. Most vibrational modes were detected for both $CpI^{[57Fe]H}$ samples that were prepared, although we did observe differences between the two samples. EPR spectroscopy revealed that the hydrogenase NRVS samples were a mixture of CpI enzymes with either oxidized (H_{ox}) or reduced (H_{red}) clusters (Figure S5). The Fe–S cluster redox states can significantly affect the energies of the Fe–S, Fe–CO, and Fe–CN vibrational modes. Thus, we discuss below the differences that we observed as well as possible assignments for some features that were not described in the main text. Further NRVS studies with the CpI enzyme as well as other [FeFe] hydrogenases, however, are required to verify the reproducibility of the ^{57}Fe normal modes and to more definitively assign them.

From the NRVS spectrum for CpI$^{[57Fe]H}$ sample #1 (Figure S4-i), we assigned the peaks at 282, 353, and 382 cm^{-1} to a ^{57}Fe-enriched [4Fe–4S]$^{2+}$ cluster since these ν(Fe–S) stretches as well as an Fe bending/breathing mode at 152 cm^{-1} were also clearly observed for the oxidized *Pf* D14C Fd. In contrast, the NRVS spectra for the [2Fe]$_H$ model complex do not show these peaks. The spectrum for CpI$^{[57Fe]H}$ sample #2 (Figure S4-ii) appears to show the same three [4Fe–4S]$^{2+}$ ν(Fe–S) modes, although their energies are slightly different (274, 359, and 377 cm^{-1}).

Additional ^{57}Fe PVDOS modes were observed at 202, 239, 269, and 298 cm^{-1} for either one or both of the CpI$^{[57Fe]H}$ samples. Similar peaks were detected for the model compounds (199, 239, 266, and 290 cm^{-1}). Therefore, it is possible that these four peaks for the hydrogenase represent Fe–S vibrations associated with the ^{57}Fe-enriched [2Fe]$_H$ subcluster. An alternative explanation is that some or all of these features may represent Fe–S modes from the hydrogenase F-domain accessory clusters, specifically the additional ^{57}Fe–S center, which we determined is not the [4Fe–4S]$_H$ subcluster.

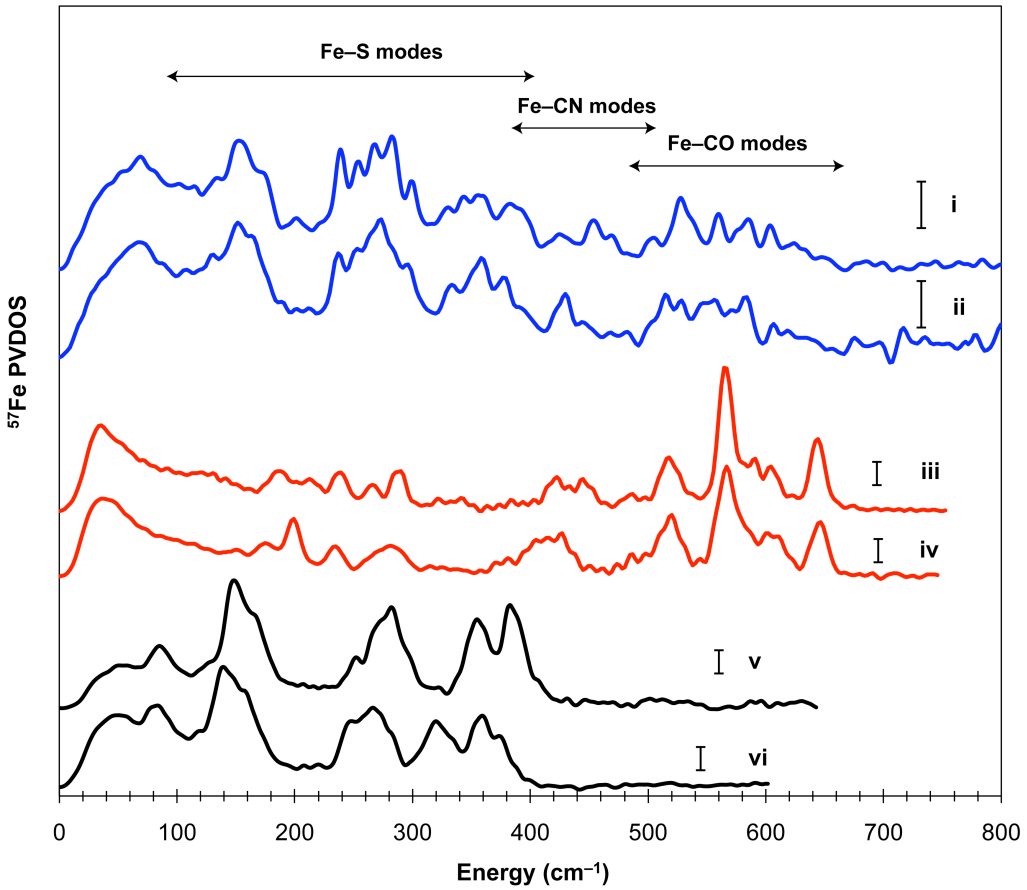

Figure S4. NRVS results for the CpI$^{[57Fe]H}$ hydrogenase compared to results from the $[^{57}Fe_2(S_2C_3H_6)(CN)_2(CO)_4]^{2-}$ model compound and a [4Fe–4S] ferredoxin. Blue curves represent the NRVS spectra for (**i**) sample 1 and (**ii**) sample 2 of the CpI$^{[57Fe]H}$ hydrogenase. Red curves are for the model complex with (**iii**) natural abundance CN^- ligands or (**iv**) isotopically labeled $^{13}CN^-$ ligands. Black curves are for the *Pf* D14C ferredoxin with (**v**) a $[4Fe–4S]^{2+}$ oxidized cluster or (**vi**) a $[4Fe–4S]^{+}$ reduced cluster. Regions are indicated where Fe–S, Fe–CO, and Fe–CN vibrational modes are expected. Vertical scale bars along the right side of each spectrum represent 30 cm for the ^{57}Fe PVDOS. The percentages of total intensity for both the Fe–S region and the Fe–CO/Fe–CN region are provided in Table S2.

Table S2. Percentage of the total ^{57}Fe PVDOS intensity for the Fe–S vibrational and Fe–CO/Fe–CN vibrational regions.

Protein	Fe–S Modes *80–400 cm^{-1}*	Fe–CO & Fe–CN Modes *400–700 cm^{-1}*
(a) CpI$^{[57Fe]H}$	75%	25%
(b) CpI$^{[57Fe]H}$	74%	26%
(c) $[^{57}Fe_2(S_2C_3H_6)(CN)_2(CO)_4]^{2-}$	47%	53%
(d) $[^{57}Fe_2(S_2C_3H_6)(^{13}CN)_2(CO)_4]^{2-}$	45%	55%
(e) *Pf* D14C Fd, oxidized	99%	1%
(f) *Pf* D14C Fd, reduced	98%	2%

Within the Fe–CO/Fe–CN region, there are several differences associated with the NRVS results for the CpI hydrogenase. For example, two Fe–CN bands were detected at 424 and 455 cm^{-1} for CpI$^{[57Fe]H}$ sample #1, while only one strong Fe–CN band was observed at 430 cm^{-1} for CpI sample #2. For both hydrogenase samples, most Fe–CO peaks have very similar energies. Results for the CpI$^{[57Fe]H}$ sample #2, however, indicate additional modes that we assign to the $[2Fe]_H$ subcluster CO ligands. These additional peaks result in a less-resolved spectrum within the higher-energy region. We believe that differences in the mixture of enzyme redox states between the two CpI$^{[57Fe]H}$ samples account for the incongruence associated with the Fe–CO and Fe–CN energies. Further studies using ^{57}Fe-enriched hydrogenase in a single redox state (e.g. only H_{ox}) will be useful to better characterize the Fe–CO and Fe–CN normal modes as measured with NRVS.

EPR spectroscopy of the CpI hydrogenase. EPR spectroscopy measurements of the CpI$^{[57Fe]H}$ samples were carried out prior to the NRVS experiments, and the results indicate that the hydrogenase samples were a mixture of proteins with different redox states (Figure S5-i). A nearly identical spectrum was previously measured for the H_2-reduced CpI hydrogenase.[13] In the pre-NRVS CpI$^{[57Fe]}$ spectrum, we identified the H_{ox} signal as well as additional lines indicative of reduced Fe–S clusters with an $S = ½$ spin state, the latter of which likely derive from accessory clusters in the reduced state and also indicate the H_{red} redox state. Although we did not include sodium dithionite in the purification buffers, and despite our attempts to oxidize CpI$^{[57Fe]H}$ with thionin, we

believe that the high concentration of enzyme (~3 mM CpI) along with the presence of H_2 in the anaerobic chamber (97% N_2 and 3% H_2) led to repeated H_2 oxidation catalyzed by the H-cluster and subsequent reduction of the F-domain ancillary clusters. After the NRVS work, the CpI$^{[57Fe]H}$ sample was thawed, diluted in buffer, and oxidized by treatment with excess thionin acetate. This generated the H_{ox} cluster as indicated by the S = ½ rhombic signal (Figure S5-ii; g_1 = 2.100, g_2 = 2.042, g_3 = 2.002). Cell-free activated CpI hydrogenase fully enriched with natural abundance Fe (i.e. CpI$^{[56Fe]H}$) was prepared and oxidized in the same manner before measuring the protein sample with EPR spectroscopy (Figure S5-iii). Spectra for both *in vitro* activated and thionin-oxidized CpI samples are identical to that of the wild-type CpI hydrogenase isolated from *Clostridium pasteurianum*.[13,14]

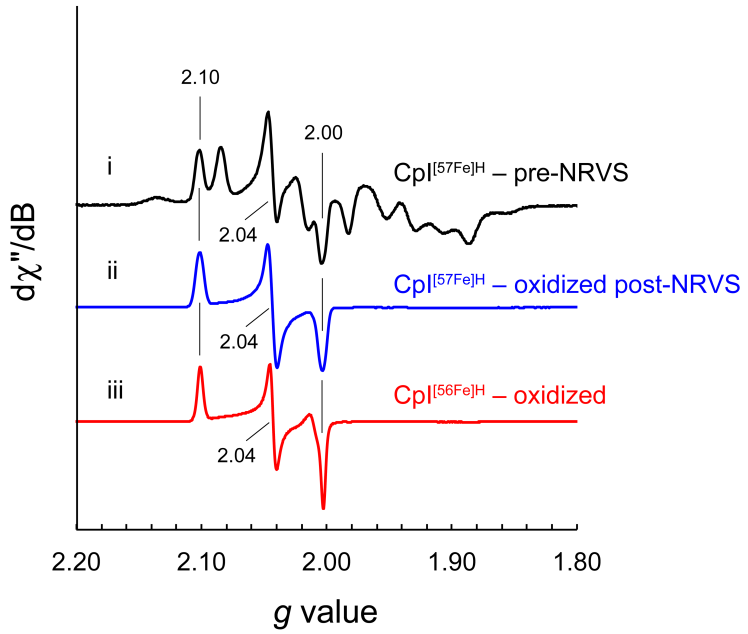

Figure S5. X-band CW EPR spectroscopy of the CpI hydrogenase. Spectra were measured at 15 K and 62 μW for (**i**) the CpI$^{[57Fe]H}$ hydrogenase before NRVS, (**ii**) CpI$^{[57Fe]H}$ oxidized with thionin acetate following NRVS, and (**iii**) non-isotopically labeled CpI$^{[56Fe]H}$ oxidized with thionin acetate. The g_1, g_2, and g_3 tensors for the S = ½ rhombic H_{ox} signal are indicated at 2.10, 2.04, and 2.00, respectively.

References

1. Mack, A. E., and Rauchfuss, T. B. (2011) (1,3-Propanedithiolato)hexacarbonyldiiron and cyanide derivatives, In *Inorganic Syntheses* (Rauchfuss, T. B., Ed.), pp 142-147.
2. Schmidt, M., Contakes, S. M., and Rauchfuss, T. B. (1999) First generation analogues of the binuclear site in the Fe-only hydrogenases: Fe2(μ-SR)2(CO)4(CN)22-, *J. Am. Chem. Soc. 121*, 9736-9737.
3. Volkers, P. I., Boyke, C. A., Chen, J., Rauchfuss, T. B., Whaley, C. M., Wilson, S. R., and Yao, H. (2008) Precursors to [FeFe]-hydrogenase models: syntheses of Fe2(SR)2(CO)6 from CO-free iron sources, *Inorg. Chem. 47*, 7002-7008.
4. Fiedler, A. T., and Brunold, T. C. (2005) Combined spectroscopic/computational study of binuclear Fe(I)-Fe(I) complexes: implications for the fully-reduced active-site cluster of Fe-only hydrogenases, *Inorg. Chem. 44*, 1794-1809.
5. Becke, A. D. (1988) Density-functional exchange-energy approximation with correct asymptotic behavior, *Phys. Rev. A 38*, 3098-3100.
6. Perdew, J. P. (1986) Density-functional approximation for the correlation energy of the inhomogeneous electron gas, *Phys. Rev. B Condens. Matter 33*, 8822-8824.
7. M. J. Frisch, G. W. T., H. B. Schlegel, G. E. Scuseria, M. A. Robb, J. R. Cheeseman, G. Scalmani, V. Barone, B. Mennucci, G. A. Petersson, H. Nakatsuji, M. Caricato, X. Li, H. P. Hratchian, A. F. Izmaylov, J. Bloino, G. Zheng, J. L. Sonnenberg, M. Hada, M. Ehara, K. Toyota, R. Fukuda, J. Hasegawa, M. Ishida, T. Nakajima, Y. Honda, O. Kitao, H. Nakai, T. Vreven, J. A. Montgomery, Jr., J. E. Peralta, F. Ogliaro, M. Bearpark, J. J. Heyd, E. Brothers, K. N. Kudin, V. N. Staroverov, R. Kobayashi, J. Normand, K. Raghavachari, A. Rendell, J. C. Burant, S. S. Iyengar, J. Tomasi, M. Cossi, N. Rega, J. M. Millam, M. Klene, J. E. Knox, J. B. Cross, V. Bakken, C. Adamo, J. Jaramillo, R. Gomperts, R. E. Stratmann, O. Yazyev, A. J. Austin, R. Cammi, C. Pomelli, J. W. Ochterski, R. L. Martin, K. Morokuma, V. G. Zakrzewski, G. A. Voth, P. Salvador, J. J. Dannenberg, S. Dapprich, A. D. Daniels, O. Farkas, J. B. Foresman, J. V. Ortiz, J. Cioslowski, D. J. Fox (2009) *Gaussian 09*, Revision A.02 ed., Gaussian, Inc, Wallingford, CT.
8. Schafer, A., Horn, H., and Ahlrichs, R. (1992) Fully optimized contracted Gaussian-basis sets for atoms Li to Kr, *J. Chem. Phys. 97*, 2571-2577.
9. Schafer, A., Huber, C., and Ahlrichs, R. (1994) Fully optimized contracted gaussian-basis sets of triple zeta valence quality for atoms Li to Kr, *J. Chem. Phys. 100*, 5829-5835.

10. Galinato, M. G. I., Whaley, C. M., and Lehnert, N. (2010) Vibrational analysis of the model complex (mu-edt)[Fe(CO)(3)](2) and comparison to iron-only hydrogenase: the activation scale of hydrogenase model systems, *Inorg. Chem. 49*, 3201-3215.
11. Guo, Y., Wang, H., Xiao, Y., Vogt, S., Thauer, R. K., Shima, S., Volkers, P. I., Rauchfuss, T. B., Pelmenschikov, V., Case, D. A., Alp, E. E., Sturhahn, W., Yoda, Y., and Cramer, S. P. (2008) Characterization of the Fe site in iron-sulfur cluster-free hydrogenase (Hmd) and of a model compound via nuclear resonance vibrational spectroscopy (NRVS), *Inorg. Chem. 47*, 3969-3977.
12. Mitra, D., Pelmenschikov, V., Guo, Y., Case, D. A., Wang, H., Dong, W., Tan, M.-L., Ichiye, T., Jenney, F. E., Adams, M. W. W., Yoda, Y., Zhao, J., and Cramer, S. P. (2011) Dynamics of the [4Fe-4S] cluster in Pyrococcus furiosus D14C ferredoxin via nuclear resonance vibrational and resonance Raman spectroscopies, force field simulations, and density functional theory calculations, *Biochemistry 50*, 5220-5235.
13. Chen, J.-S., and Mortenson, L. E. (1976) In *Iron and Copper Proteins* (Yasunobu, K. T., Mower, H. F., and Hayaishi, O., Eds.), pp 68-82, Plenum Press, New York.
14. Adams, M. W., and Mortenson, L. E. (1984) The physical and catalytic properties of hydrogenase II of Clostridium pasteurianum. A comparison with hydrogenase I, *J. Biol. Chem. 259*, 7045-7055.